MOLECULAR AND CELLULAR BIOLOGY, June 2000, p. 4275–4287 Vol. 20, No. 12
0270-7306/00/$04.00+0

Disruption of the 11-*cis*-Retinol Dehydrogenase Gene Leads to Accumulation of *cis*-Retinols and *cis*-Retinyl Esters

CAROLA A. G. G. DRIESSEN,[1]* HUUB J. WINKENS,[1] KIRSTIN HOFFMANN,[2] LEONOOR D. KUHLMANN,[1] BERT P. M. JANSSEN,[1] ANKE H. M. VAN VUGT,[1] J. PRESTON VAN HOOSER,[3] B. E. WIERINGA,[4] AUGUST F. DEUTMAN,[1] KRZYSZTOF PALCZEWSKI,[3,5,6] KLAUS RUETHER,[2] AND JACQUES J. M. JANSSEN[1]

Department of Ophthalmology, University of Nijmegen, 6525 EX Nijmegen, The Netherlands[1]; Department of Ophthalmology, Humboldt University, 15553 Berlin, Germany[2]; Departments of Ophthalmology,[3] Chemistry,[5] and Pharmacology,[6] University of Washington, Seattle, Washington 98195; and Department of Cell Biology, University of Nijmegen, 6500 HB Nijmegen, The Netherlands[4]

Received 28 January 2000/Accepted 13 March 2000

To elucidate the possible role of 11-*cis*-retinol dehydrogenase in the visual cycle and/or 9-*cis*-retinoic acid biosynthesis, we generated mice carrying a targeted disruption of the 11-*cis*-retinol dehydrogenase gene. Homozygous 11-*cis*-retinol dehydrogenase mutants developed normally, including their retinas. There was no appreciable loss of photoreceptors. Recently, mutations in the 11-*cis*-retinol dehydrogenase gene in humans have been associated with fundus albipunctatus. In 11-*cis*-retinol dehydrogenase knockout mice, the appearance of the fundus was normal and punctata typical of this human hereditary ocular disease were not present. A second typical symptom associated with this disease is delayed dark adaptation. Homozygous 11-*cis*-retinol dehydrogenase mutants showed normal rod and cone responses. 11-*cis*-Retinol dehydrogenase knockout mice were capable of dark adaptation. At bleaching levels under which patients suffering from fundus albipunctatus could be detected unequivocally, 11-*cis*-retinol dehydrogenase knockout animals displayed normal dark adaptation kinetics. However, at high bleaching levels, delayed dark adaptation in 11-*cis*-retinol dehydrogenase knockout mice was noticed. Reduced 11-*cis*-retinol oxidation capacity resulted in 11-*cis*-retinol/13-*cis*-retinol and 11-*cis*-retinyl/13-*cis*-retinyl ester accumulation. Compared with wild-type mice, a large increase in the 11-*cis*-retinyl ester concentration was noticed in 11-*cis*-retinol dehydrogenase knockout mice. In the murine retinal pigment epithelium, there has to be an additional mechanism for the biosynthesis of 11-*cis*-retinal which partially compensates for the loss of the 11-*cis*-retinol dehydrogenase activity. 11-*cis*-Retinyl ester formation is an important part of this adaptation process. Functional consequences of the loss of 11-*cis*-retinol dehydrogenase activity illustrate important differences in the compensation mechanisms between mice and humans. We furthermore demonstrate that upon 11-*cis*-retinol accumulation, the 13-*cis*-retinol concentration also increases. This retinoid is inapplicable to the visual processes, and we therefore speculate that it could be an important catabolic metabolite and its biosynthesis could be part of a process involved in regulating 11-*cis*-retinol concentrations within the retinal pigment epithelium of 11-*cis*-retinol dehydrogenase knockout mice.

Upon illumination of rhodopsin, the chromophore 11-*cis*-retinal is isomerized to all-*trans*-retinal, which is subsequently released from the protein. Enzymes involved in the regeneration of 11-*cis*-retinal are part of the visual cycle (28). Two redox reactions are known to play a role in this cycle (48). One of these reactions is the reduction of all-*trans*-retinal to all-*trans*-retinol, catalyzed by retinol dehydrogenases present in the photoreceptor cells. A second reaction is the oxidation of 11-*cis*-retinol to 11-*cis*-retinal in the retinal pigment epithelium (RPE).

Simon and coworkers and we previously reported the cloning of a retinol dehydrogenase highly expressed in the RPE (4, 37, 38). Recombinant retinol dehydrogenase catalyzes stereospecific oxidation of 11-*cis*-retinol but not all-*trans*-retinol. The enzyme, which belongs to the superfamily of short-chain alcohol dehydrogenases, was referred to as 11-*cis*-retinol dehydrogenase (11-*cis*-RoDH). Recently, two additional short-chain alcohol dehydrogenases were cloned that recognize 11-*cis*-retinol as a substrate, called CRAD1 and CRAD2 (*cis*-retinol/androgen dehydrogenase type 1 and type 2, respectively) (2, 41). These enzymes are expressed at high levels in the liver and at low levels in the RPE. CRAD1 is also highly expressed in the kidney. Like CRAD1 and CRAD2, expression of 11-*cis*-RoDH is also widely distributed, because 11-*cis*-RoDH transcripts were detected in several other ocular and nonocular tissues in adults (6, 22, 42). Mouse embryos at gestation day 10-11 also display a broad expression pattern of 11-*cis*-RoDH (32). This raises questions about the relative significance of these three enzymes in the visual cycle and their functional role in general retinoid metabolism elsewhere. Several independent studies have shown that recombinant 11-*cis*-RoDH mediates the oxidation of 9-*cis* and 13-*cis* isomers of retinol (6, 22, 35, 42). Moreover, 11-*cis*-RoDH was found to be able to use 5α-androstan-3α, 17β-diol, and andosterone as substrates (42), suggesting that 11-*cis*-RoDH may have a broader biological significance than anticipated originally.

In the last decade, many proteins have been identified which cause retinal degeneration. Among these are proteins that function in the phototransduction cascade, have a structural role in the rod photoreceptor, or are involved in retinoid metabolism (serum retinol-binding protein, cellular retinaldehyde-binding protein, and RPE65) (8, 18, 21, 24, 36; for an overview, see Retnet at www.sph.uth.tmc.edu). Mice in which those

* Corresponding author. Mailing address: Department of Ophthalmology, University of Nijmegen, Philips van Leijdenlaan 15, 6525 EX Nijmegen, The Netherlands. Phone: 31243615160. Fax: 31243540522. E-mail: c.driessen@ohk.azn.nl.

genes were disrupted have compromised retinal structures and functions (9, 16, 17, 31, 44, 47). Recently, mutations in the 11-*cis*-RoDH gene were found in two patients with fundus albipunctatus (46). Here we report on the generation and characterization of a mouse model in which the 11-*cis*-RoDH gene is disrupted. Novel data were obtained that support a role for this enzyme in the visual cycle and unravel an interesting compensatory mechanism in mouse eyes that partially compensates for the lack of 11-*cis*-RoDH gene product.

MATERIALS AND METHODS

Construction of the targeting vector. The murine 11-*cis*-RoDH gene was isolated from a 129/Sv mouse genomic library (6). A restriction map of the gene is shown in Fig. 1. A multiple cloning site containing *Not*I, *Nhe*I, *Eco*RI, *Sal*I, *Kpn*I, *Bam*HI, and *Hin*dIII restriction sites was subcloned into the pgem13zf(+) vector (Promega, Leiden, The Netherlands). A 2.6-kb *Eco*RI fragment spanning the 11-*cis*-RoDH gene from −3155 to −568 was cloned into the *Bam*HI site, while a second fragment of the 11-*cis*-RoDH gene, spanning from +1955 to +5728, was cloned into the *Kpn*I site. The 1.2-kb neomycin resistance gene cassette was isolated as an *Xho*I fragment and cloned into the vector using the *Sal*I site. Homologous recombination would result in elimination of the −568 to +1955 region of the 11-*cis*-RoDH gene, which includes exons I, II, and III of this gene. Another gene, called *GCN5L1*, is present upstream (637 nucleotides) of the 11-*cis*-RoDH gene (5). The *GCN5L1* gene was not affected by the described targeting disruption strategy. The targeting vector was linearized with *Not*I.

Generation of chimeric mice. Embryonic stem (ES) cells (129/Sv) were cultured on irradiated SNLH9 feeder cell layers. After electroporation of the targeting vector, cells were cultured in selective medium containing 350 μg of neomycin (G418) per ml and 0.2 μM FIAU. To check appropriate targeting, Southern blot analysis were performed. A 1.2-kb *Nhe*I fragment flanking the 5′ end of the targeting vector was used as a probe to detect a 9.2-kb *Bam*HI fragment derived from the wild-type allele and a 6.1-kb *Bam*HI fragment from the targeted allele. The 3′-flanking region was checked using a 0.6-kb probe (obtained by genomic PCR with the upstream primer 5′-TGAGAATTCCTAG TTGGC-3′ and downstream primer 5′-TTTTCAATTAAACGGATT-3′), which detected a 9.5-kb *Sst*I fragment derived from the wild-type allele and an 8.2-kb *Sst*I fragment from the targeted allele. Before microinjection, selected ES cell lines were subjected to karyotype analysis. Three cell lines were finally used for microinjection into 3.5-day-old C57BL/6 mouse blastocysts. Injected blastocysts were implanted into pseudopregnant C57BL/6 foster mothers. Chimeric male mice were mated with C57BL/6 females. Agouti offspring were analyzed for heterozygous pups by Southern blot analysis (as described above) or PCR. For PCR analysis, two primers, KORDH-s1 (5′-GGGCAGCTGCAGTCTGCACC ATC-3′, upstream primer located in exon IV of the *GCN5L1* gene), and neo-a1 (5′-GCCCCGACTGCATCTGCGTGTT-3′, downstream primer located in the neomycin cassette) were used. The presence of a targeted allele was revealed by amplification of a 365-bp fragment. Heterozygotes were crossed to generate wild-type (11-*cis*-RoDH$^{+/+}$), heterozygous (11-*cis*-RoDH$^{+/-}$), and homozygous (11-*cis*-RoDH$^{-/-}$) offspring. These three genotypes were also characterized by PCR. For PCR analysis, two primers, KORDH-s1 and KORDH-a1 (5′-GGGC AAGACCTGACCTGGGGGC-3′, located in intron III of the 11-*cis*-RoDH gene) were used. From the targeted allele, a 1.5-kb fragment was amplified, while from the wild-type allele a 2.9-kb fragment was amplified.

11-*cis*-RoDH RT-PCR. For reverse transcriptase-PCR (RT-PCR), total RNA was isolated from whole eyes and kidneys of 11-*cis*-RoDH$^{+/+}$, 11-*cis*-RoDH$^{+/-}$, and 11-*cis*-RoDH$^{-/-}$ mice and subsequently reverse transcribed to obtain cDNA. The primer sets used in these procedures are: 11-*cis*-RoDH, sense (5′-ATGTGGCTGCCTCTGCTTCT-3′) and antisense (5′-CCAGAGCAGCTTGG CATCCC-3′) or sense (5′-TTCTTTCGAACCCCTGTGAC-3′) and antisense (CCAGAGCAGCTTGGCATCCC-3′); opsin, sense (5′-GTCGGCTGGTCCA GGTAC-3′) and antisense (5′-GCCACAGCAGAGAGTGGTG-3′); and actin, sense (5′-ATGGGTCAGAAGGACTCCTA-3′) and antisense (5′-TTGATGTC ACGCACGATTTC-3′). Product sizes were 0.9 and 0.25 kb for 11-*cis*-RoDH, respectively, 0.25 kb for opsin, and 0.5 kb for actin.

Rhodopsin assay. Mice were dark adapted for 16 h. All further experiments were performed under dim red light. Mice were killed, and their eyes were removed. Each eye was homogenized in 2 ml of phosphate-buffered saline (PBS, pH 7.4). Homogenates were centrifuged at 145,000 × *g* and 4°C for 20 min, and the pellets were resuspended in 1 ml of 1% Triton X-100–PBS. Samples were incubated for 1 h at 4°C and subsequently centrifuged at 145,000 × *g* and 4°C for 20 min. Supernatants were analyzed by UV/VIS spectroscopy. Before the absorbance spectra were measured, 20 μM hydroxylamine (pH 6.5) was added to each sample. To quantitate the amount of rhodopsin, a dark spectrum from 700 to 250 nm was recorded first. To obtain a bleached spectrum, samples were illuminated for 5 min with a 100-W light bulb at a distance of 10 cm. Prior to illumination, samples were placed behind a KG1 heat filter (Schott, Mainz, Germany). Difference spectra (illuminated spectrum subtracted from the dark spectrum) were used for accurate quantification of the rhodopsin content per eye using an extinction coefficient of 42,000 mol/liter per cm.

Retinoid extraction and analysis. Retinoid analysis was performed under dim red light as described previously with some modifications (29). In brief, dark-adapted animals were kept in the dark for 16 h, whereas light-adapted animals were kept in the dark for 16 h and subsequently exposed to light (200 cd/m^2) for 90 min in their cages. Animals were sacrificed by cervical dislocation. Eyes were collected, snap frozen in foil-wrapped Eppendorf tubes on dry ice-ethanol, and stored at −80°C. Anterior segments of collected eyes were removed, and the remaining, still-frozen, posterior segments were homogenized with 1 ml of 0.1 M MOPS (morpholinepropanesulfonic acid, pH 6.5) containing 10 mM NH_2OH and 0.2% sodium dodecyl sulfate (SDS). ^{3}H-labeled all-*trans*-retinol (200,000 dpm) was added in order to determine the extraction yield of retinoids. The suspension was homogenized ~10 times and incubated for 30 min at room temperature to convert retinals to oximes. For retinoid extraction, the suspension was mixed with 1 ml of absolute ethanol and 4 ml of hexane. Suspensions were shaken vigorously at room temperature for 2 min, and phase separation was subsequently achieved by centrifugation (4,000 rpm, 5 min, 4°C). The upper phase was collected, and the extraction was repeated on the lower phase. Extracted retinoids were dried under argon and resolved in 300 μl of hexane at room temperature.

Retinoid analysis was performed on an HP 1100 series high-pressure liquid chromatograph (HPLC) equipped with a diode array detector and HP Chemstation A.04.05 software, allowing identification of retinoid isomers according to their specific retention time and absorption maxima. A normal-phase, narrow-bore column (Alltech Silica 5u Solvent Miser, 2.1 by 250 mm) and an isocratic solvent composed of 4% ethyl acetate in hexane at a flow rate of 0.5 ml/min were used to separate retinyl esters from 11-*cis*-retinal, all-*trans*-retinal, 11-*cis*-retinol, and all-*trans*-retinol at room temperature. Retinyl esters were collected and saponified to determine the isomeric composition of the ester pool. The solvent from HPLC fractions encompassing the retinyl esters (typically 500 μl) was evaporated under argon. Retinyl esters were dissolved in 230 μl of absolute ethanol and hydrolyzed with 20 μl of 6 M KOH for 30 min at 55°C. To extract the products, the sample was diluted with 100 μl of water, chilled on ice for 2 min, and extracted with 300 μl of hexane. Hydrolyzed extracted retinoids were analyzed directly by HPLC as described above. 11-*cis*-Retinol and 13-*cis*-retinol were separated on a Beckman Ultrasphere Silica 5u column with 1.5% dioxane in hexane at a flow rate of 1.4 ml/min at 20°C. 11-*cis*- and 13-*cis*-retinol were eluted after ~43 and ~45 min, respectively. To determine spontaneous isomerization of retinols, we spiked RPE bovine membranes with isomerically pure retinols. Spiked membranes were incubated for 30 min to allow formation of retinyl esters. The esters were extracted and subjected to a procedure similar to that described above in order to determine the extent of nonspecific isomerization due to sample handling. These control experiments showed that under the conditions used to determine the isomeric composition of retinyl esters mentioned above, ~16% of the added 11-*cis*-retinol isomerizes to 13-*cis*- and ~33% isomerizes to all-*trans*-retinol.

ERG recordings. Electroretinograms (ERGs) were recorded on 11-*cis*-RoDH$^{+/+}$, 11-*cis*-RoDH$^{+/-}$, and 11-*cis*-RoDH$^{-/-}$ mice (six of each) at the age of 3 months. Anesthesia was induced by subcutaneous injection of 20 mg of xylazine plus 40 mg of ketamine per kg of body weight. Pupils were dilated with 1% atropine and 0.5% tropicamide. ERGs were recorded using a monopolar electrode with a plastic speculum and an embedded wire loop (diameter, 3 mm) and two subcutaneously applied silver needles: 3 mm below the eye as a reference and in the forehead as a ground electrode. Methylcellulose was put on the plastic speculum in order to obtain a tight connection between electrode and eye. Each mouse was placed in a Ganzfeld bowl (Toennies Multiliner Vision, Hoechberg, Germany). Signals were digitized at a rate of 1.7 kHz. The Ganzfeld stimulus was characterized by a duration of ~50 μs and a white flash color temperature of 6,000 K.

For scotopic ERGs, mice were dark adapted for 2 h. The flash intensities used ranged from 4×10^{-4} to 2.5 cd m^{-2}, divided into eight steps of 0.4 or 0.6 log cd m^{-2}. At the four lower intensities, five responses were averaged (interstimulus interval, 2 s), whereas at higher intensities two responses were recorded (interstimulus interval, 5 s). Immediately after the scotopic ERG recordings, mice were exposed to a background light of 30 cd m^{-2} for 10 min in order to obtain photopic ERGs. A single flash response was obtained with 15 cd m^{-2} (digitizing rate, 2.56 kHz; gain, 25,000; average, 16).

For dark adaptation ERGs, two approaches were applied. The first approach was characterized by conditions under which human patients suffering from fundus albipunctatus could be detected unequivocally. The mice were dark-adapted for 2 h. Subsequently the maximal scotopic ERG response was recorded using a 100-mcd m^{-2} stimulus. Bleaching was obtained using 100 cd of white light per m^2 for 2 min. Over a 20-min period, the ERG response was recorded every minute using a flash intensity of 100 mcd m^{-2}. The responses were not averaged to avoid light adaptation. In a second experimental setup, we wanted to bleach a much higher amount of rhodopsin. After a 16-h period of dark adaptation, an ERG response using a 100-mcd m^{-2} stimulus was recorded. The animals were subsequently exposed to 800 cd m^{-2} for 10 min. Experimental conditions are partly derived from those described previously for analysis of dark adaptation kinetics in rhodopsin transgenic mice (7). After the light had been turned off, the 100-mcd m^{-2} stimulus was delivered every 3 min. The endpoint of observation was set at 45 min because a single maximal dose of anesthesia was given, allowing us to keep the animals sedated for 1 h. All procedures adhered to the standards

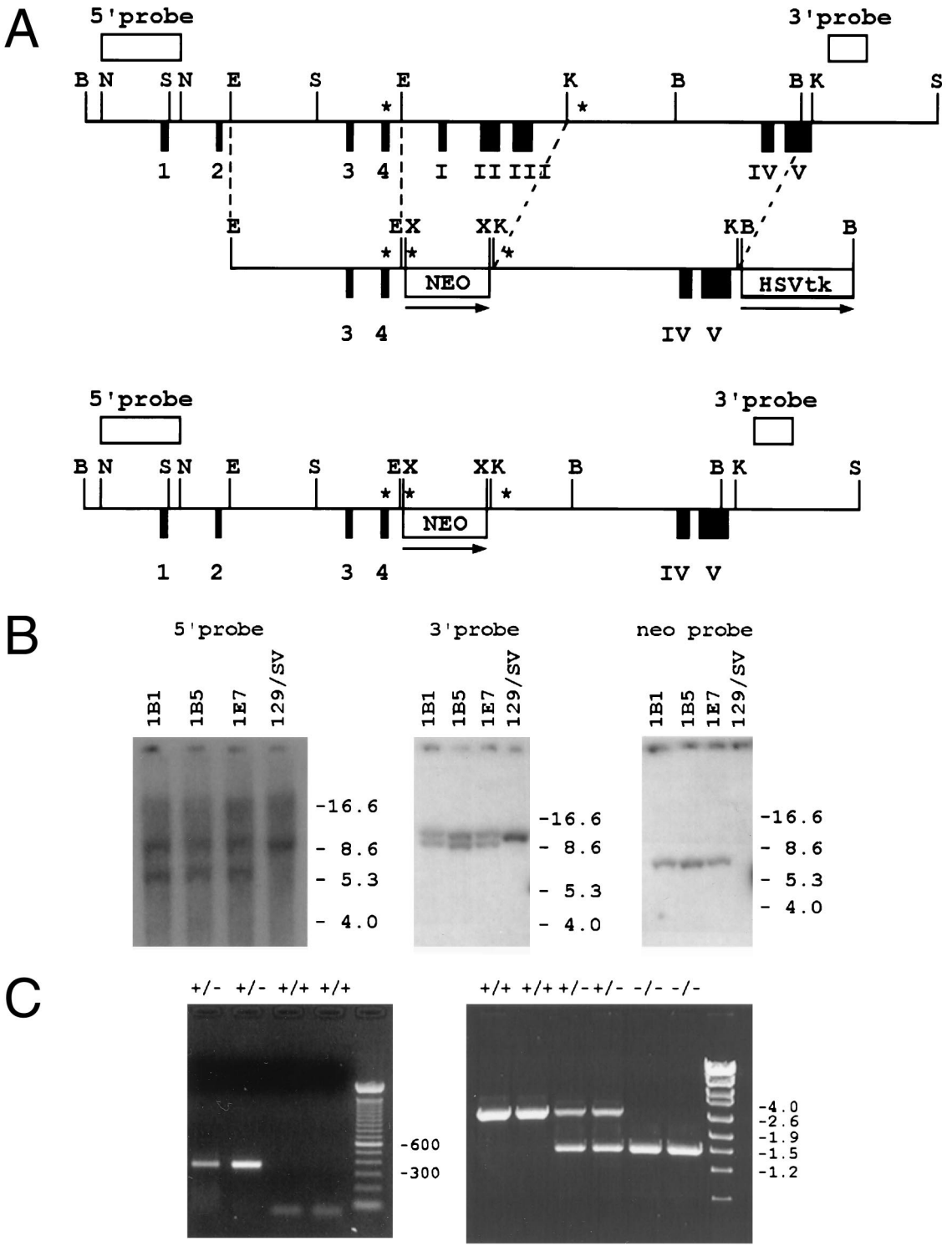

FIG. 1. Gene targeting of the murine 11-*cis*-RoDH gene. (A) Genomic structures of the murine 11-*cis*-RoDH (roman numbers) and *GCN5L1* (arabic numbers) genes (upper panel), structure of the targeting vector (middle panel), and genomic structure of the targeted 11-*cis*-RoDH gene (lower panel). Homologous recombination results in the replacement of exons I, II, and III of the 11-*cis*-RoDH gene by a neomycin cassette (NEO). Positions of the 5′ and 3′ probes are indicated. Asterisks mark positions of the primers used for PCR genotype analysis. Abbreviations: B, *Bam*HI; E, *Eco*RI; K, *Kpn*I; N, *Nhe*I; S, *Sst*I; HSVtk, herpes simplex virus thymidine kinase gene. (B) Southern blot analysis of the cell lines. Autoradiograms of three Southern blots containing genomic DNA from three targeted ES cell lines and from mouse strain 129/Sv after hybridization with the 5′ probe (left), 3′ probe (middle), or *neo* probe (right). Sizes are shown in kilobases. (C) PCR genotyping of mouse tail DNA. PCR fragments derived from wild-type (11-*cis*-RoDH$^{+/+}$), heterozygous (11-*cis*-RoDH$^{+/-}$), and homozygous (11-*cis*-RoDH$^{-/-}$) mice. Offspring were analyzed with primers KORDH-s1 and neo-a1. The presence of a targeted allele results in the amplification of a 365-bp fragment (left panel). Offspring from 11-*cis*-RoDH$^{+/-}$ parents were analyzed with primers KORDH-s1 and KORDH-a1, which results in fragments of 2.9 kb in 11-*cis*-RoDH$^{+/+}$ mice, 1.5 and 2.9 kb in 11-*cis*-RoDH$^{+/-}$ mice, and 1.5 kb in 11-*cis*-RoDH$^{-/-}$ mice (right panel).

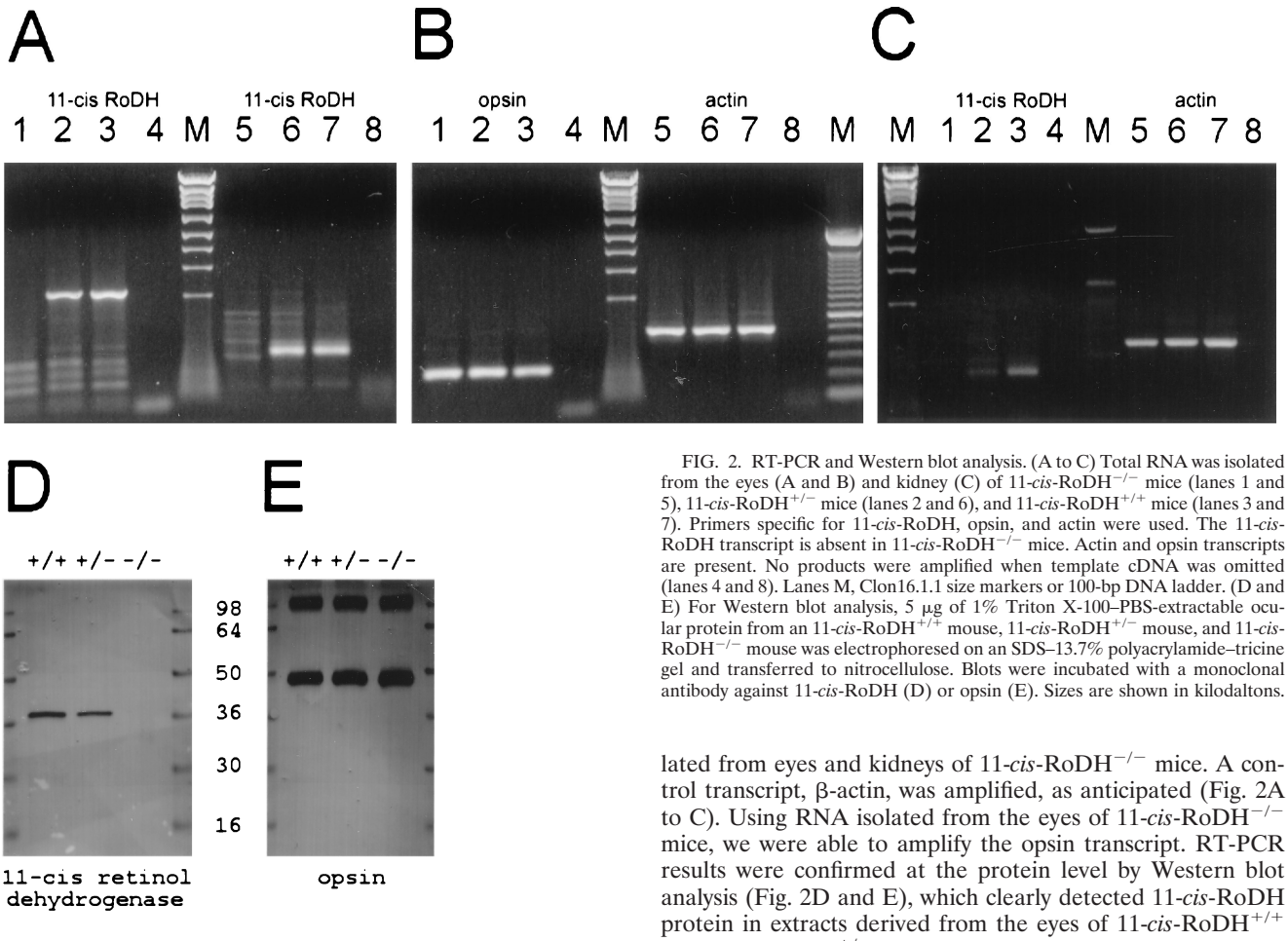

FIG. 2. RT-PCR and Western blot analysis. (A to C) Total RNA was isolated from the eyes (A and B) and kidney (C) of 11-*cis*-RoDH$^{-/-}$ mice (lanes 1 and 5), 11-*cis*-RoDH$^{+/-}$ mice (lanes 2 and 6), and 11-*cis*-RoDH$^{+/+}$ mice (lanes 3 and 7). Primers specific for 11-*cis*-RoDH, opsin, and actin were used. The 11-*cis*-RoDH transcript is absent in 11-*cis*-RoDH$^{-/-}$ mice. Actin and opsin transcripts are present. No products were amplified when template cDNA was omitted (lanes 4 and 8). Lanes M, Clon16.1.1 size markers or 100-bp DNA ladder. (D and E) For Western blot analysis, 5 μg of 1% Triton X-100–PBS-extractable ocular protein from an 11-*cis*-RoDH$^{+/+}$ mouse, 11-*cis*-RoDH$^{+/-}$ mouse, and 11-*cis*-RoDH$^{-/-}$ mouse was electrophoresed on an SDS–13.7% polyacrylamide–tricine gel and transferred to nitrocellulose. Blots were incubated with a monoclonal antibody against 11-*cis*-RoDH (D) or opsin (E). Sizes are shown in kilodaltons.

set by the animal ethics committee of the Humboldt University in Berlin. The criterion for successful dark adaptation for 11-*cis*-RoDH$^{+/+}$ mice was defined as the time point when reproducible ERG responses comparable to the prebleach recording could be observed or was set at 45 min for 11-*cis*-RoDH$^{-/-}$ mice. For statistical analysis of the ERG data on single cone responses and also for the time point analysis of the dark adaptation, the *t* test was applied.

RESULTS

Construction of 11-*cis*-RoDH knockout mice. The strategy used to target and inactivate the 11-*cis*-RoDH gene by replacement of exons 1 to 3 is outlined in Fig. 1A. ES cells that had undergone a correct targeting event were identified by examining 213 G418-resistant clones by Southern blot analysis (Fig. 1B). Three cell lines with a normal karyotype were selected for use in blastocyst injection and embryo transfer into foster mothers. Among the offspring, five chimeric males (20 to 60% Agouti coat color) and three chimeric females (20 to 30% Agouti coat color) were identified. Germ line-transmitting males were selected by following segregation of the mutant allele with PCR (Fig. 1C). Heterozygous offspring were interbred to generate wild-type (11-*cis*-RoDH$^{+/+}$), heterozygous (11-*cis*-RoDH$^{+/-}$), and homozygous (11-*cis*-RoDH$^{-/-}$) mice. The offspring were genotyped using a second PCR strategy, allowing identification of three genotypes in a single assay (Fig. 1C).

Analysis of 11-*cis*-RoDH expression. RT-PCR analysis were performed on total RNA isolated from whole eyes or kidneys of 11-*cis*-RoDH$^{+/+}$, 11-*cis*-RoDH$^{+/-}$, and 11-*cis*-RoDH$^{-/-}$ mice. No 11-*cis*-RoDH transcript was detected in RNA isolated from eyes and kidneys of 11-*cis*-RoDH$^{-/-}$ mice. A control transcript, β-actin, was amplified, as anticipated (Fig. 2A to C). Using RNA isolated from the eyes of 11-*cis*-RoDH$^{-/-}$ mice, we were able to amplify the opsin transcript. RT-PCR results were confirmed at the protein level by Western blot analysis (Fig. 2D and E), which clearly detected 11-*cis*-RoDH protein in extracts derived from the eyes of 11-*cis*-RoDH$^{+/+}$ and 11-*cis*-RoDH$^{+/-}$ mice but not in ocular protein extracts of 11-*cis*-RoDH$^{-/-}$ mice (10).

Retinal structure, rhodopsin content, and fundus appearance. To investigate the role of 11-*cis*-RoDH in retinal development, eyes from 7-day-old animals were used for histology (Fig. 3A and B). The thickness of the retina appeared to be the same in all three genotypes. Moreover, all retinal layers were present in both 11-*cis*RoDH$^{+/-}$ and 11-*cis*-RoDH$^{-/-}$ mice. At the light-microscopic level, no disturbances within the retina were observed when 11-*cis*-RoDH$^{+/-}$ and 11-*cis*-RoDH$^{-/-}$ mice were compared with 11-*cis*-RoDH$^{+/+}$ animals. Immunohistochemistry showed the presence of 11-*cis*-RoDH in the RPE of 11-*cis*-RoDH$^{+/+}$ and 11-*cis*-RoDH$^{+/-}$ mice, while 11-*cis*-RoDH was absent in 11-*cis*-RoDH$^{-/-}$ mice (data not shown). The eyes of 2-, 6-, and 9-month-old animals were examined to analyze a possible role of 11-*cis*-RoDH in retinal degeneration. No differences between the three genotypes were observed at the age of 2 months (Fig. 3C and D) and 6 months (Fig. 3E and F). There was also no indication of retinal pathology at the age of 9 months (data not shown).

The eyes of dark-adapted 11-*cis*-RoDH$^{+/+}$, 11-*cis*-RoDH$^{+/-}$, and 11-*cis*-RoDH$^{-/-}$ mice contained 0.58 ± 0.05, 0.57 ± 0.05, and 0.59 ± 0.03 nmol of rhodopsin per eye, respectively. Additionally, 11-*cis*-RoDH$^{+/+}$, 11-*cis*-RoDH$^{+/-}$, and 11-*cis*-RoDH$^{-/-}$ mice were placed under constant light (200 cd/m^2 for 90 min). Three animals were sacrificed at the end of this period. The remaining animals were placed in the dark for 5, 60, and 120 min. The data presented in Fig. 4 show that maximal rhodopsin levels were reached by all three genotypes

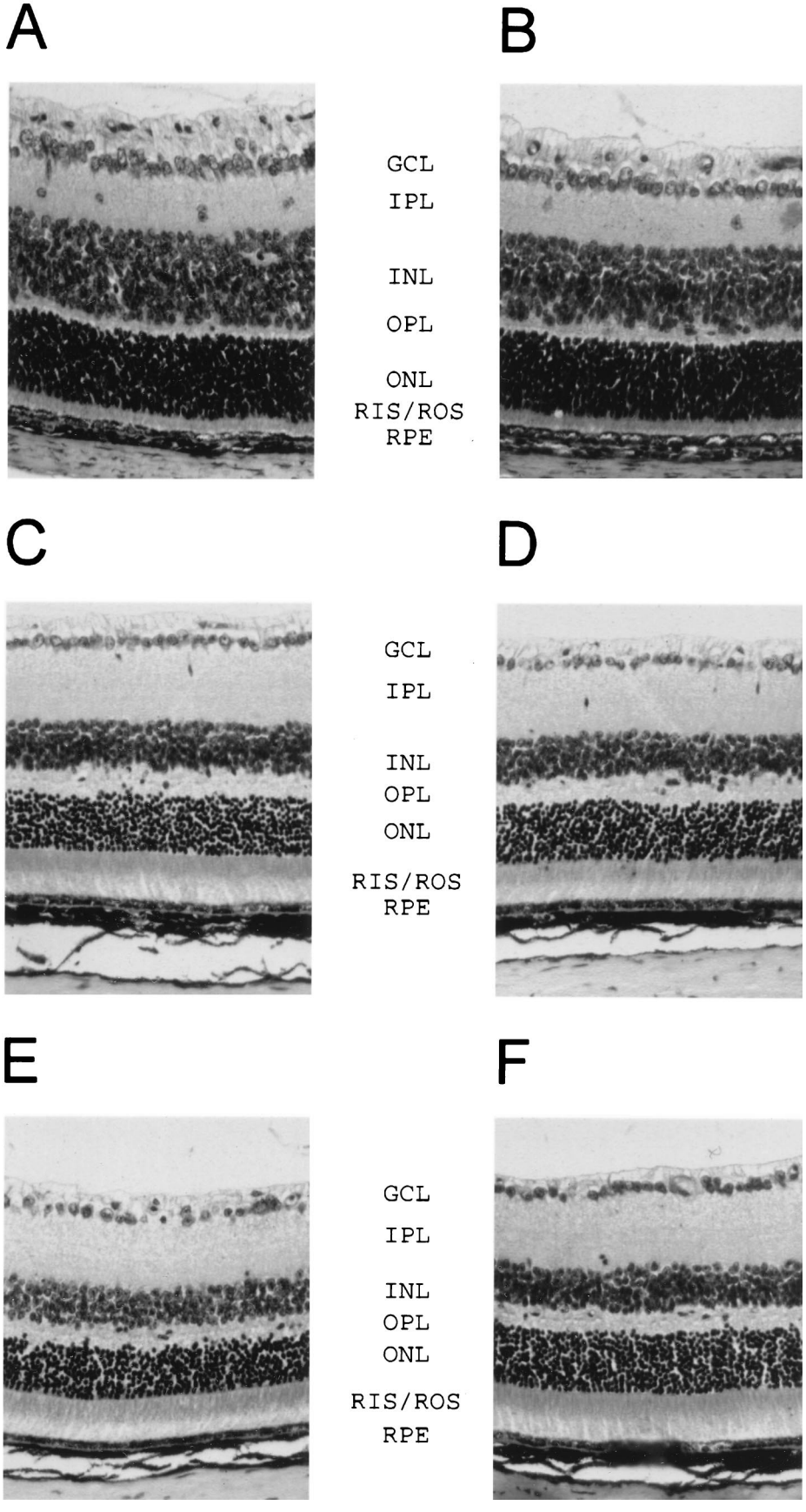

FIG. 3. Retinal morphology. Retinal sections were obtained from 11-*cis*-RoDH$^{-/-}$ (A, C, and E) and 11-*cis*-RoDH$^{+/+}$ (B, D, and F) mice aged 7 days (A and B), 2 months (C and D), and 6 months (E and F). RPE, retinal pigment epithelium; ROS, rod outer segment; RIS, rod inner segment; ONL, outer nuclear layer; OPL, outer plexiform layer; INL, inner nuclear layer; IPL, inner plexiform layer; GCL, ganglion cell layer.

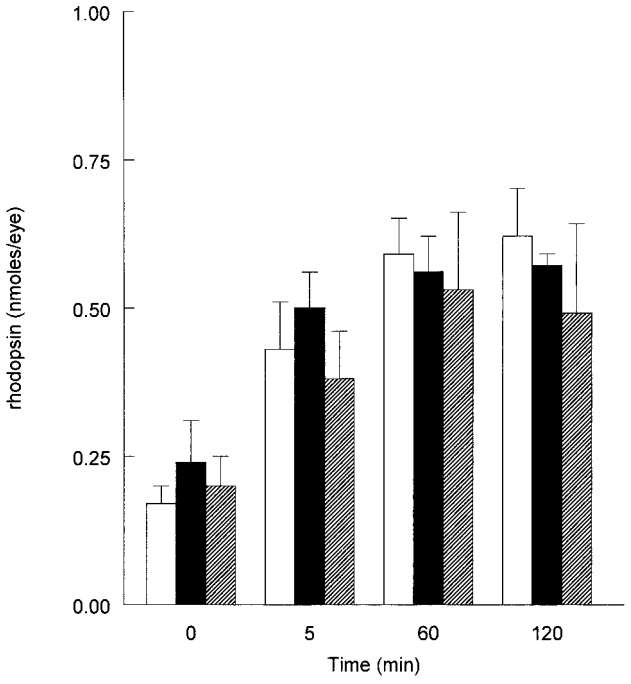

FIG. 4. Bleaching and recovery of rhodopsin. 11-*cis*-RoDH$^{+/+}$ (open bars), 11-*cis*-RoDH$^{+/-}$ (solid bars), and 11-*cis*-RoDH$^{-/-}$ (hatched bars) mice were given continuous light with an intensity of 200 cd/m^2 for 90 min. Following this light period, ±65% of the visual pigment was bleached. Animals that were dark-adapted for 16 h were found to contain 0.58 ± 0.05 (11-*cis*-RoDH$^{+/+}$, mean ± SD, n = 3), 0.57 ± 0.05 (11-*cis*-RoDH$^{+/-}$, mean ± SD, n = 3), and 0.59 ± 0.03 (11-*cis*-RoDH$^{-/-}$, mean ± SD, n = 3) nmol of rhodopsin per eye. Data presented show that that these levels are reached by all three genotypes tested within a 60-min period. Under these conditions there is no clear difference between the regeneration rates of 11-*cis*-RoDH$^{+/+}$ (7.5 ± 1.5 pmol/min), 11-*cis*-RoDH$^{+/-}$ (5.3 ± 1.9 pmol/min), and 11-*cis*-RoDH$^{-/-}$ (5.5 ± 1.4 pmol/min) mice.

within a 60-min period. These studies suggested that the rate of rhodopsin recovery in 11-*cis*-RoDH$^{+/+}$ mice was somewhat faster than in 11-*cis*-RoDH$^{-/-}$ mice. However, we never observed a significant difference between the regeneration rates of 11-*cis*-RoDH$^{+/+}$ (7.5 ± 1.5 pmol/min), 11-*cis*-RoDH$^{+/-}$ (5.3 ± 1.9 pmol/min), and 11-*cis*-RoDH$^{-/-}$ (5.5 ± 1.4 pmol/min) mice.

Fundus albipunctatus belongs to a group of retinopathies characterized by a flecked retina. To investigate whether 11-*cis*-RoDH$^{-/-}$ mice also have white punctata present in their fundus, video ophthalmoscopy was performed with a scanning laser ophthalmoscope. There was no difference between the fundus of 11-*cis*-RoDH$^{+/+}$ and 11-*cis*-RoDH$^{-/-}$ mice. As an example, Fig. 5A and B show two fundus photographs of 2-month-old 11-*cis*-RoDH$^{+/+}$ and 11-*cis*-RoDH$^{-/-}$ mice, respectively. The retinal pigment epithelia are smooth, blood vessels show no irregularities and, moreover, no white punctata are present.

Retinoid analysis. The animals used in these studies were housed under 12-h dark conditions and were ~3 months old. Before the eyes were collected for retinoid analysis, mice were dark adapted for 16 h. Three animals were sacrificed in the dark (dark adapted) and three received 200 cd/m^2 for 90 min (light adapted). The posterior segments of these eyes were collected and prepared for retinoid analysis.

In Fig. 6, typical HPLC separation profiles are presented for retinoids extracted from the dark-adapted eyes of 11-*cis*-RoDH$^{+/+}$ and 11-*cis*-RoDH$^{+/-}$ (Fig. 6A) and 11-*cis*-RoDH$^{-/-}$ (Fig. 6B) mice. Because of 11-*cis*-RoDH enzymatic properties in vitro, increased 11-*cis*-retinol concentrations in 11-*cis*-RoDH$^{-/-}$ mice were expected. Eyes derived from 11-*cis*-RoDH$^{-/-}$ mice contained 49 ± 22 pmol of 11-*cis*-retinol plus 13-*cis*-retinol per eye (mean ± standard error of the mean [SEM], n = 3), compared to 7 ± 0.9 pmol (mean ± SEM, n = 3) in 11-*cis*-RoDH$^{+/+}$ mice (Fig. 6A versus B; see also Table 1). Small amounts of these retinols and large differences in their absorption coefficients did not allow precise estimation of the 11-*cis*-retinol:13-*cis*-retinol ratio. Rough estimation based on the spectrum suggests an equal molar ratio of these isomers. Although not visible in the chromatogram, a large increase in the retinyl ester concentration in the eyes of 11-*cis*-RoDH$^{-/-}$ mice was observed in both dark- and light-adapted eyes (Tables 1 and 2). To determine the isomeric composition, retinyl esters were collected and saponified. Typical results are shown in Fig. 6A′ for 11-*cis*-RoDH$^{+/+}$ and Fig. 6B′ for 11-*cis*-RoDH$^{-/-}$ mice. There was a large increase in the ratio of *cis*-retinyl esters to all-*trans*-retinyl esters in the eyes derived from dark-adapted 11-*cis*-RoDH$^{-/-}$ mice (Fig. 6A′ versus B′).

UV/VIS spectroscopy and coelution with authentic retinoid standards were used to identify the retinoids. For example, retinoids present in peak 5 had a λ_{max} at 325 nm (inset in Fig. 6A′), and their retention time corresponded perfectly to that of the all-*trans*-retinol standard. Looking at the spectra of peaks 4, we noticed some heterogeneity (inset, Fig. 6B′), resulting in a λ_{max} of between 319 and 330 nm, which suggests a mixture of 11-*cis*-retinol and 13-*cis*-retinol isomers. 13-*cis*-Retinol is spontaneously formed at room temperature, and thus it was necessary to estimate the extent of this reaction using synthetic standards. Separation of 11-*cis*- and 13-*cis*-retinol was achieved in 1.5% dioxane in hexane. In addition to a ~4-fold increase observed in the ester concentration in 11-*cis*-RoDH$^{-/-}$ mice (Tables 1 and 2), we also observed a change in the isomeric composition of the ester pool (Tables 3 and 4). Analysis shows a ~50-fold increase in *cis*-retinyl ester concentrations in the eyes of dark-adapted 11-*cis*-RoDH$^{-/-}$ mice. In dark-adapted 11-*cis*-RoDH$^{-/-}$ eyes, 73.2% ± 2.4% (mean ± SEM, n = 3) is present as 11-*cis*-retinyl esters and 13-*cis*-retinyl esters, compared to only 6.8% ± 3.4% (mean ± SEM, n = 3) in dark-adapted 11-*cis*-RoDH$^{+/+}$ eyes. Approximately 25% of the total esters are present as the 11-*cis* isomer (Table 3). A smaller but significant increase in the *cis*-retinyl ester concentration in dark-adapted eyes of 11-*cis*-RoDH$^{+/-}$ mice was also noticed. Other retinoids were similar to those in 11-*cis*-RoDH$^{+/+}$ mice. The concentration of 11-*cis*-retinal in all three genotypes is comparable to the concentration of rhodopsin, as described above, suggesting that this retinal is coupled almost exclusively with opsin. The retinyl ester composition in eyes of 11-*cis*-RoDH$^{+/+}$ mice did not change significantly following light adaptation bleaching ~60% of the rhodopsin present. In 11-*cis*-RoDH$^{+/-}$ and 11-*cis*-RoDH$^{-/-}$ eyes, 11-*cis*-retinyl esters were depleted to <2% and ~10%, respectively, as a result of light adaptation. Light also caused depletion of free *cis*-retinols in 11-*cis*-RoDH$^{-/-}$ eyes.

ERG recordings. When mice were 3 months old, ERGs of 11-*cis*-RoDH$^{+/+}$, 11-*cis*-RoDH$^{+/-}$, and 11-*cis*RoDH$^{-/-}$ mice were recorded at increasing stimulus intensities under dark-adapted conditions. As a typical example, we show the original scotopic ERG recordings of an 11-*cis*-RoDH$^{+/+}$ mouse and 11-*cis*-RoDH$^{-/-}$ mouse in Fig. 7A and B, respectively. A difference between 11-*cis*-RoDH$^{+/+}$ mice and 11-*cis*-RoDH$^{+/-}$ was not observed, and the results for 11-*cis*-RoDH$^{+/-}$ mice are therefore not shown. There is no statistical difference between the scotopic ERG b-wave amplitudes of 11-*cis*-RoDH$^{-/-}$ and 11-*cis*-RoDH$^{+/+}$ animals after 2 h of dark adaptation at all

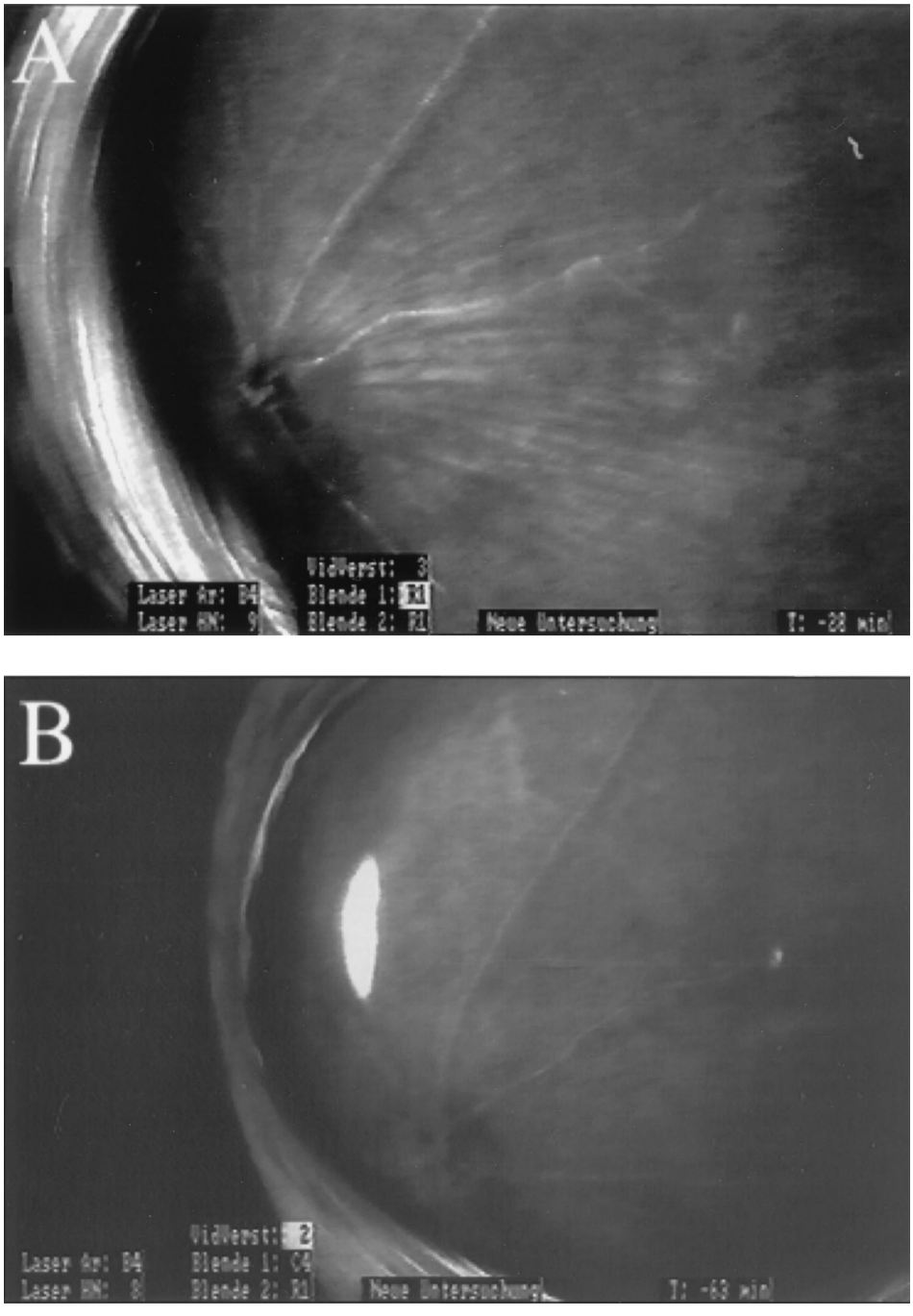

FIG. 5. Scanning laser ophthalmoscope photographs of 11-*cis*-RoDH$^{+/+}$ (A) and 11-*cis*-RoDH$^{-/-}$ (B) mice at the age of 2 months.

intensities tested. The amplitudes for the 11-*cis*-RoDH$^{-/-}$ mice tend to be even higher. Interestingly, we also noticed higher concentrations of 11-*cis*-retinal in 11-*cis*-RoDH$^{-/-}$ eyes of fully dark-adapted animals (Table 1). The ERG response under dark-adapted conditions is mainly derived from rod activity, and hence, rod photoreceptor cells in 11-*cis*-RoDH$^{-/-}$ mice seem to be fully functional. At 7 months of age, there was still no difference between the ERG recordings of 11-*cis*-RoDH$^{-/-}$ and 11-*cis*-RoDH$^{+/+}$ animals (data not shown).

The photopic ERGs were recorded after the scotopic ERG recordings and a light adaptation period (30 cd m^{-2}) of 10 min. It was assumed that mainly cones contribute to the ERG response when a background light of 30 cd m^{-2} and a flash intensity of 15 cd m^{-2} is used. As an example, Fig. 7C and D show the photopic ERG recordings of an 11-*cis*-RoDH$^{+/+}$ mouse and an 11-*cis*-RoDH$^{-/-}$ mouse, respectively, at the age of 3 months. Using the *t* test, there is no statistical difference between the cone single-response amplitudes of 11-*cis*-RoDH$^{-/-}$ and 11-*cis*-RoDH$^{+/+}$ mice ($P = 0.44$). Hence, in addition to the rod photoreceptor cells, the cone photoreceptor cells are also fully functional in 11-*cis*-RoDH$^{-/-}$ mice.

Yamamoto and coworkers reported on mutations in the

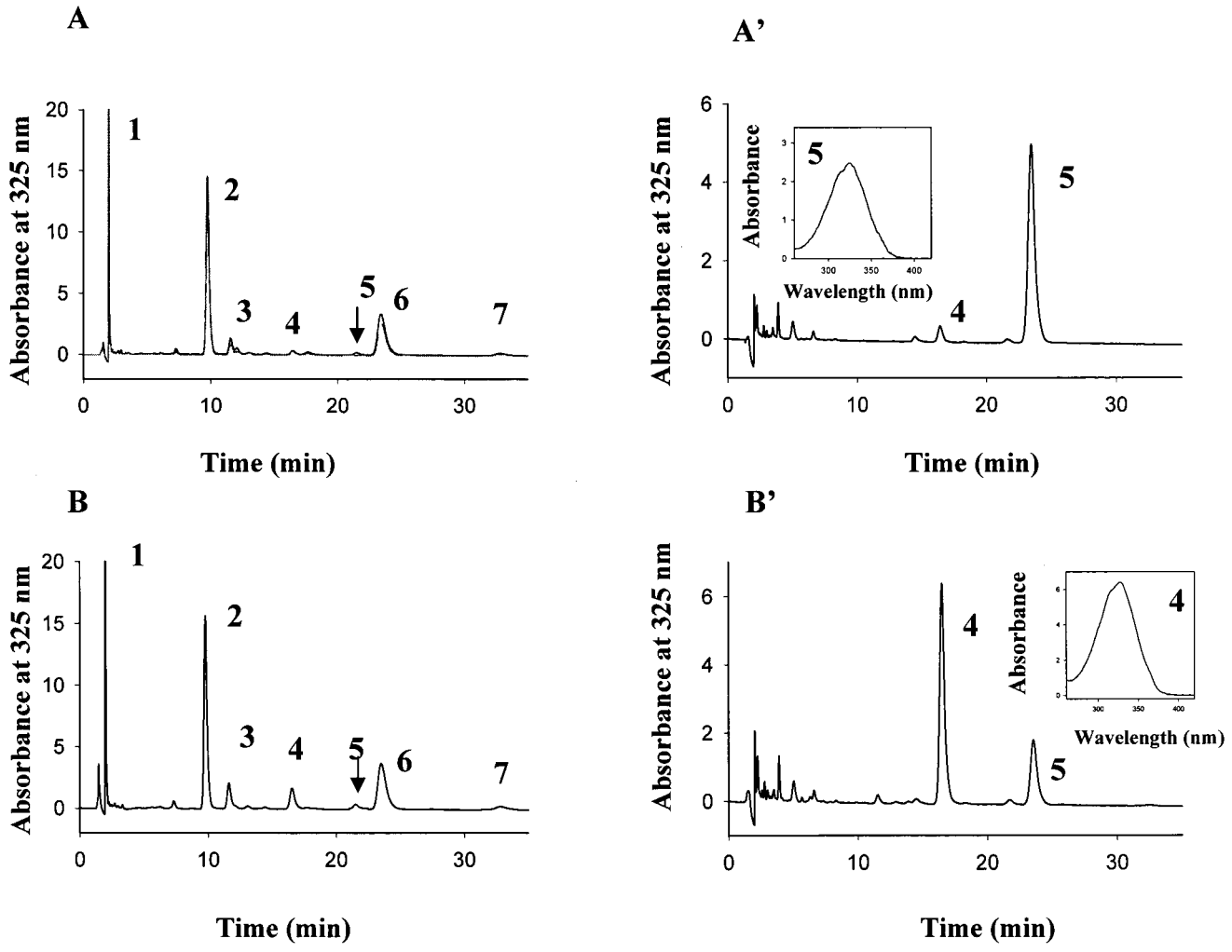

FIG. 6. 11-*cis*-RoDH mouse ocular retinoid analysis. (A) Typical chromatogram of retinoid separation for 11-*cis*-RoDH$^{+/+}$ and 11-*cis*-RoDH$^{+/-}$ mice. Note that both chromatograms are very similar and were superimposed. Peaks: 1, retinyl esters; 2 and 6, *anti*- and *syn*-11-*cis*-retinal oximes; 3 and 7, *anti*- and *syn*-all-*trans*-retinal oximes; 5, all-*trans*-retinol; 4, 11-*cis*-retinol plus 13-*cis*-retinol. (B) Typical chromatogram of retinoid separation for 11-*cis*-RoDH$^{-/-}$ mice. (A′ and B′) Analysis of isomeric composition of retinyl esters obtained for 11-*cis*-RoDH$^{+/+}$ and 11-*cis*-RoDH$^{-/-}$ mice, respectively. Insets: UV/VIS spectra of peaks 5 and 4, respectively.

11-*cis*-RoDH gene of patients suffering from fundus albipunctatus (46). Fundus albipunctatus patients have normal scotopic and photopic ERG responses but suffer from abnormal dark adaptation kinetics. They often reach normal ERG amplitudes only after a prolonged period of dark adaptation. To look for this effect, five 11-*cis*-RoDH$^{-/-}$ mice and five control mice were dark adapted for 2 h and bleached with 100 cd m^{-2} for 2 min. After the light was turned off, the ERG was recorded every minute for 20 min with a flash intensity of 100 mcd m^{-2}. Under these conditions, the onset time and amplitude of the b-waves were not statistically different between 11-*cis*-RoDH$^{-/-}$ and 11-*cis*-RoDH$^{+/+}$ mice, both reaching a maximal amplitude after ~18 min. A typical example is shown in Fig. 8A (11-*cis*-RoDH$^{+/+}$) and B (11-*cis*-RoDH$^{-/-}$). The experiment was modified by using a longer period of dark adaptation and a higher bleaching level. After 16 h of dark adaptation, a pre-bleach scotopic ERG was recorded (Fig. 8C, D, and E) and the anesthetized animals were subsequently light adapted for 10

TABLE 1. Retinoid analysis of dark-adapted mice

11-*cis*-RoDH type	Mean amt (pmol/eye) ± SD				
	Retinyl esters	11-*cis*-Retinal	All-*trans*-retinal	11-*cis*-Retinol/13-*cis*-retinol	All-*trans*-retinol
+/+	145 ± 41	465 ± 47	37 ± 5	7 ± 0.9	5 ± 3
+/−	255 ± 118	504 ± 31	47 ± 4	8.5 ± 0.5	6 ± 4
−/−	699 ± 224	589 ± 33	60 ± 26	49 ± 22	2 ± 1

TABLE 2. Retinoid analysis of light-adapted mice

11-*cis*-RoDH type	Mean amt (pmol/eye) ± SD				
	Retinyl esters	11-*cis*-Retinal	All-*trans*-retinal	11-*cis*-Retinol/13-*cis*-retinol	All-*trans*-retinol
+/+	104 ± 21	145 ± 37	210 ± 25	7 ± 1.9	75 ± 3
+/−	394 ± 35	198 ± 30	201 ± 30	11 ± 1.5	38 ± 4
−/−	422 ± 58	218 ± 9	218 ± 9	30 ± 8	46 ± 3

TABLE 3. Isomeric composition of esters in dark-adapted mice

11-*cis*-RoDH type	% of total esters		
	All-*trans*-retinyl	11-*cis*-Retinyl plus 13-*cis*-retinyl	11-*cis*-Retinyl
+/+	93 ± 3.4	6.8 ± 3.4	<2
+/−	81 ± 6.5	18.5 ± 6.5	~8
−/−	26 ± 2.4	73.2 ± 2.4	~25

TABLE 4. Isomeric composition of esters in light-adapted mice

11-*cis*-RoDH type	% of total esters		
	All-*trans*-retinyl	11-*cis*-Retinyl plus 13-*cis*-retinyl	11-*cis*-Retinyl
+/+	95 ± 1.0	4.9 ± 1.0	<2
+/−	94 ± 3.4	5.7 ± 0.4	<2
−/−	46 ± 2.4	54 ± 0.8	~10

min with an 800-cd m^{-2} background. Over a 45-min period, a single ERG response was recorded every 3 min using a white flash of 100 mcd m^{-2} (Fig. 8F, G, and H show typical examples). In control animals, a reproducible response emerged after a mean time period of 18 ± 3 min (mean ± standard deviation [SD], $n = 9$) compared to >45 min ($n = 8$) in 11-*cis*-RoDH$^{-/-}$ animals. Using the *t* test, the difference in dark adaptation kinetics observed between 11-*cis*-RoDH$^{-/-}$ and 11-*cis*-RoDH$^{+/+}$ mice was found to be highly significant ($P > 0.0001$). Data show delayed dark adaptation in 11-*cis*-RoDH$^{-/-}$ mice, provided a considerable amount of rhodopsin is bleached.

DISCUSSION

General consequences because of 11-*cis*-RoDH function loss. This report describes the construction of an 11-*cis*-RoDH knockout animal model. The 11-*cis*-RoDH enzyme was found to be capable of catalyzing the oxidation of *cis*-isomers of retinol, including 11-*cis*-, 9-*cis*-, and 13-*cis*-retinol (4, 6, 22, 37, 42). Oxidation of 9-*cis*-retinol to 9-*cis*-retinaldehyde is likely to be the first step in the 9-*cis*-retinoic acid (RA) biosynthesis pathway. RA plays an important role in differentiation, apoptosis, and reproduction by regulating gene transcription through interaction with retinoid receptors, several of which

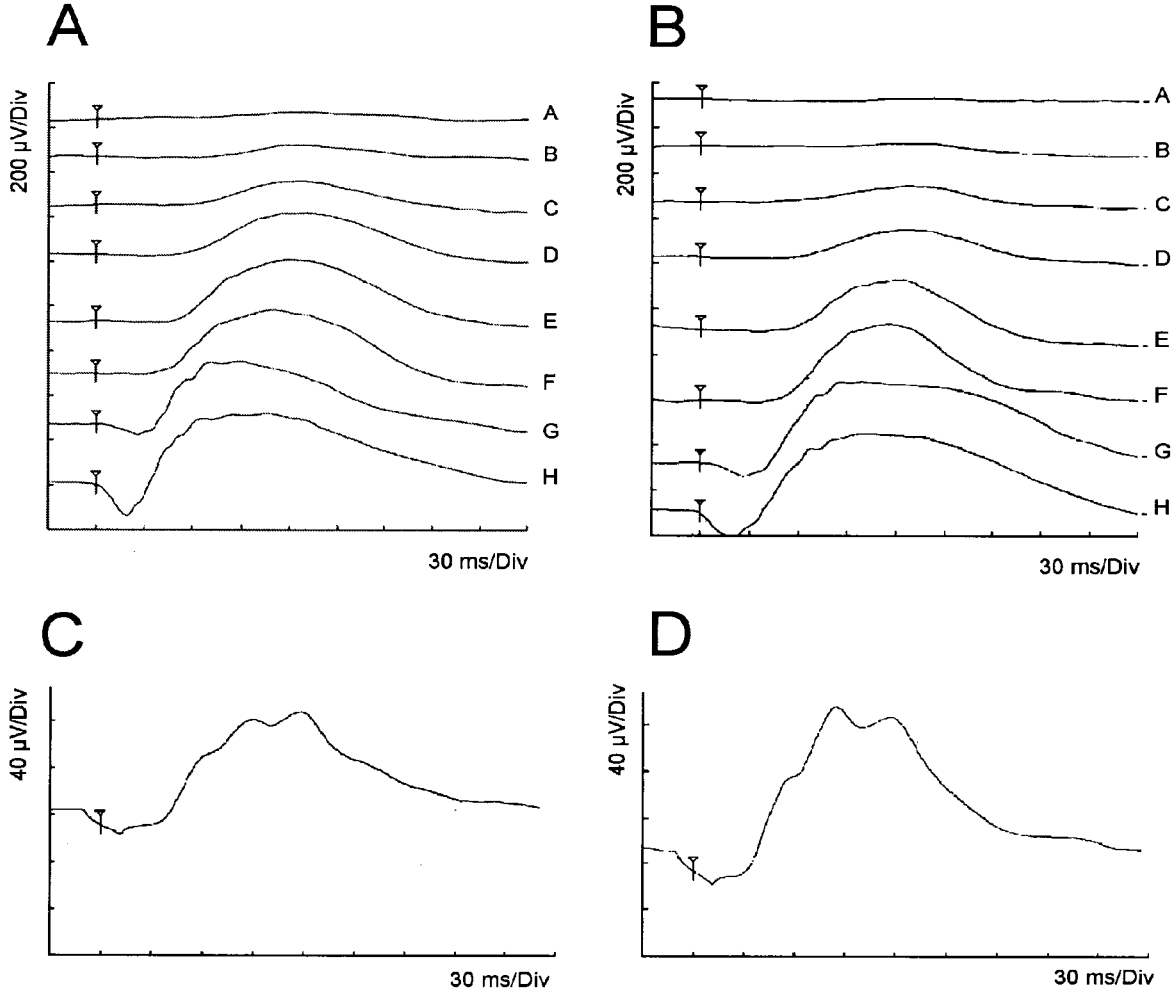

FIG. 7. ERG analysis. Scotopic ERG recordings (A and B) and photopic ERG recordings (C and D) of a 3-month-old 11-*cis*-RoDH$^{+/+}$ mouse (A and C) and a 3-month-old 11-*cis*-RoDH$^{-/-}$ mouse (B and D). The onset of the flash is indicated by open triangles. For scotopic ERGs the flash intensities used were 0.04 (A), 0.1 (B), 0.4 (C), 1.0 (D), 4.0 (E), 10.0 (F), 100.0 (G), and 1,000 (H) mcd m^{-2}. For photopic ERGs, mice were exposed to a background light of 30 cd m^{-2} for 10 min. A single flash response was obtained with 15 cd m^{-2}.

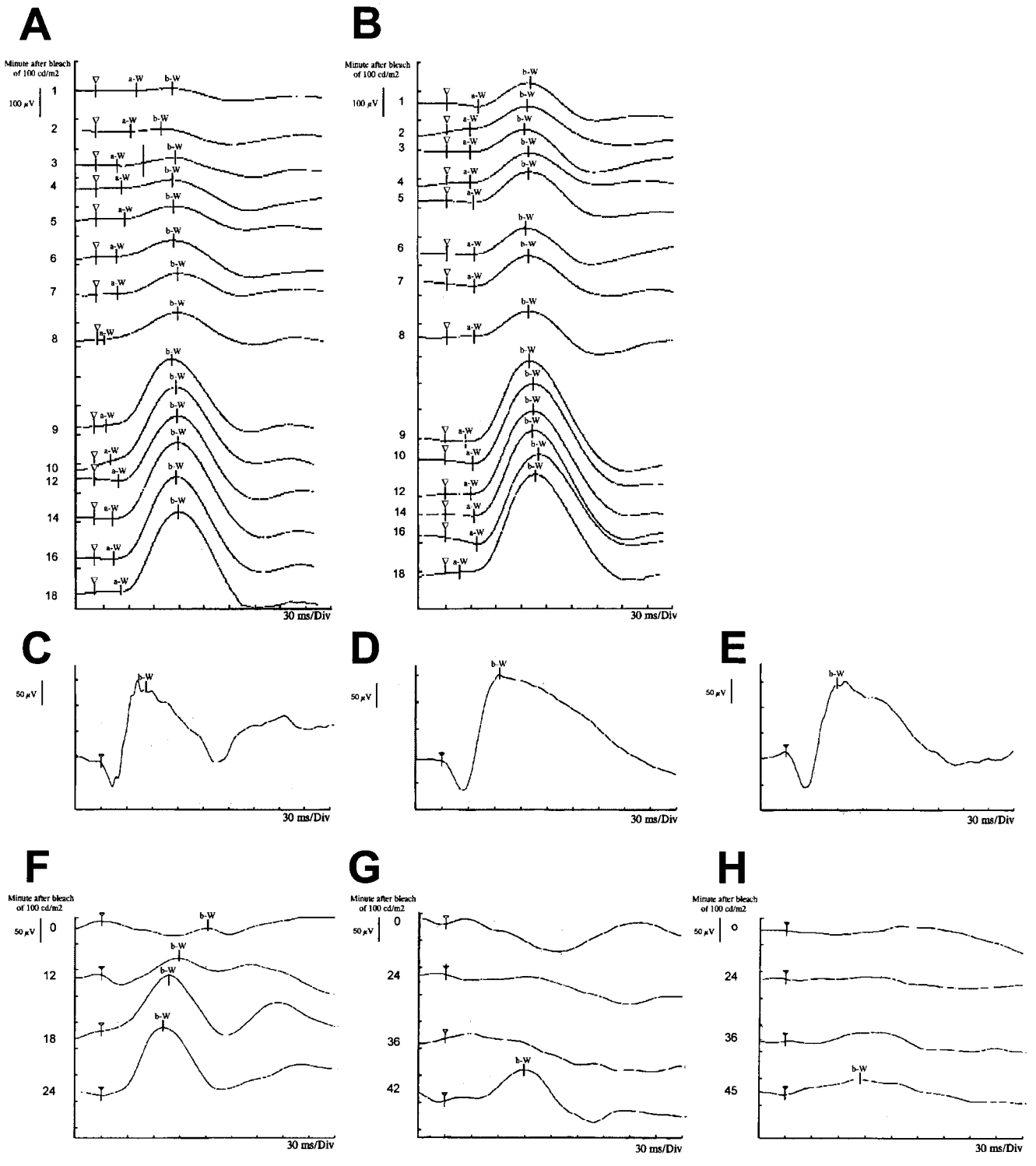

FIG. 8. Dark adaptation. Mice were dark adapted for 2 h and bleached for 2 min using 100 cd m^{-2} (A and B). Scotopic ERGs were recorded every minute during a 20-min period using a flash intensity of 10^{-1} cd m^{-2}. B-wave amplitudes of 11-*cis*-RoDH$^{-/-}$ animals (B) compared to 11-*cis*-RoDH$^{+/+}$ animals (A) were not delayed. To achieve a higher level of bleaching, animals were dark adapted for 16 h and bleached for 10 min using 800 cd m^{-2}. A prebleaching ERG using a flash of 10^{-1} cd m^{-2} was recorded (C, D, and E). After the bleach an ERG was recorded again using a flash of 10^{-1} cd m^{-2} every 3 min (F, G, and H). In all 11-*cis*-RoDH$^{+/+}$ mice, an ERG was recorded after ~18 min (F, typical example) similar to the prebleach ERG. After 18 min, no ERG could be detected in any of the 11-*cis*-RoDH$^{-/-}$ mice (G and H). Two 11-*cis*-RoDH$^{-/-}$ mice started to respond after 42 min (G), but most 11-*cis*-RoDH$^{-/-}$ mice did not respond after 45 min (H), by which time we had to terminate the experiment for reasons mentioned in the text.

are present in the (pre)mature vertebrate retina (3, 11, 27, 43). Romert and coworkers found that the murine 11-*cis*-RoDH gene is transcribed in embryonic tissues as early as gestation day 9 (32), which, taken together with its substrate specificity, hints at involvement of 11-*cis*-RoDH in prenatal development through 9-*cis*-RA biosynthesis. However, 11-*cis*-RoDH turned out not to be essential for embryonic development and viability. This shows that 11-*cis*-RoDH is possibly not involved in 9-*cis*-RA biosynthesis prenatally or 9-*cis*-RA is not essential for embryonic development or 11-*cis*-RoDH$^{-/-}$ mice can compensate for the loss of 11-*cis*-RoDH activity. Wang and coworkers showed that the enzyme could be involved in 5α-androstan-3α, 17β-diol, and andosterone metabolism and therefore might influence fertility (42). However, both female and male 11-*cis*-RoDH$^{-/-}$ mice were found to be fertile, and moreover, 11-*cis*-RoDH$^{-/-}$ couples gave birth to ~50% female and 50% male offspring. In conclusion, the data thus far did not present us with evidence for a crucial role of 11-*cis*-RoDH in the 9-*cis*-RA biosynthetic pathway or steroid metabolism in vivo.

Visual cycle in 11-*cis*-RoDH$^{-/-}$ mice. A striking phenotypic characteristic of 11-*cis*-RoDH$^{-/-}$ mice is overproduction of 11-*cis*-retinol, accumulating as a free alcohol and in the form of retinyl esters. Lack of 11-*cis*-RoDH did not affect production of 11-*cis*-retinal, suggesting that another oxidizing system is taking over for the production of this important aldehyde. Indeed, using a combination of NAD and NADP, we recently postulated the presence of an additional NADP-dependent oxidizing system in RPE (35). In mice, the absence of 11-*cis*-RoDH could be compensated for by a higher concentration of its substrate, 11-*cis*-retinol. A higher 11-*cis*-retinol concentration might be necessary if, for example, a second oxidation system is less efficient (high K_m) in production of 11-*cis*-retinal. High-level production of 11-*cis*-retinol upon disruption of the visual cycle complex might be the result of deinhibition of an enzyme(s) involved in the isomerization of all-*trans*-retinol to 11-*cis*-retinol.

The isomerization of all-*trans*-retinol to 11-*cis*-retinol occurs enzymatically without an exogenous source of energy (1). Hydrolysis of all-*trans*-retinyl carboxylic ester provides the 4 kcal/mol energy needed for isomerization, and retinyl esters were proposed to be essential intermediates in 11-*cis*-retinol formation. More recently, Winston and Rando (45) proposed that 11-*cis*-retinol (and to a lesser degree 13-*cis*-retinol) is a very potent inhibitor of isomerization. This observation would explain why 11-*cis*-RoDH$^{+/+}$ mice do not complete conversion of all-*trans*-retinyl esters to 11-*cis*-retinyl esters (see, for example, Fig. 6) in this putative exothermic reaction. However, as shown in Fig. 6, 11-*cis*-RoDH$^{-/-}$ mice overproduce 11-*cis*-retinol and 11-*cis*-retinyl esters, suggesting that isomerization could occur in vivo even in the presence of high 11-*cis*-retinol or 11-*cis*-retinyl ester levels. Hence, overproduction of 11-*cis*-retinol in 11-*cis*-RoDH$^{-/-}$ mice did not inhibit conversion of all-*trans*-retinyl esters but was, on the contrary, found to increase formation of 11-*cis*-retinoids.

This isomerization model has been challenged recently (40). It was proposed that apo-CRALBP or another binding system of 11-*cis*-retinol appears to be necessary in vitro to monitor isomerase activity. A similar mechanism might operate in vivo. The retinoid-binding proteins that drive the reaction may overcome the thermodynamically unfavorable isomerization reaction. In this model, all-*trans*-retinol or an unidentified retinyl intermediate participates in the isomerization reaction. Formed 11-*cis*-retinol is oxidized to 11-*cis*-retinal and saturates the binding sites (driving force for isomerization). The consequence of isomerization proceeding only in the presence of the acceptor protein(s) would be that an 11-*cis*-retinal pool does not accumulate in RPE because it is only formed on demand. Lack of sufficient 11-*cis*-retinol oxidation capacity could result in overproduction of unbound 11-*cis*-retinol because it binds to CRALBP with lower affinity than 11-*cis*-retinal (33). The system would try to establish a new equilibrium, and higher levels of 11-*cis*-retinyl esters could be a way of reaching this equilibrium. The 11-*cis*-RoDH$^{-/-}$ mice behave as predicted by this model. Hence, the availability of mice with disrupted 11-*cis*-RoDH activity will be very useful to obtain additional insights into the isomerization reaction.

An unexpected observation was the high level of 13-*cis*-retinyl esters in 11-*cis*-RoDH$^{-/-}$ mice. 11-*cis*-RoDH is a promiscuous enzyme toward *cis*-isomers of retinols (6, 22, 35, 42). Purified enzyme reduces both 11-*cis*- and 13-*cis*-retinal with similar efficiency (K_m, 4.6 and 4.4 μM; respectively; V_{max}, 568 and 440 nmol/min per mg with NADH, respectively; G.-F. Jang, K. Palczewski, and F. Haeseleer, unpublished). In fact, the dehydrogenase is somewhat more efficient towards 11-*cis*- and 13-*cis*-retinal than 9-*cis*-retinal (2.2 μM and 130 nmol/min per mg). Because 13-*cis*-retinol is formed spontaneously at ambient temperature and has no known physiological function, it is likely that a mechanism which strives to remove this analog from circulation is present. This may be even more the case in a tissue like the retina, which experiences high fluxes of retinoids. The lack of 11-*cis*-RoDH in RoDH$^{-/-}$ mice for the first time reveals in vivo accumulation of 13-*cis*-retinol, for the major part in the form of esters. These observations raise many questions regarding the metabolism of 13-*cis*-retinol. The generated knockout animals are useful for elucidating further details of this process.

11-*cis*-RoDH-deficient mice as a model of fundus albipunctatus. Under normal environmental conditions, 11-*cis*-RoDH knockout mice did not display white punctata resembling those observed in the fundus of fundus albipunctatus patients. Punctata are present from the day of birth and show no or little progression during a patient's lifetime. It is likely that the flecked retina typical of fundus albipunctatus patients results from a developmental defect. This is likely to be caused by a role of 11-*cis*-RoDH in RA biosynthesis. RA was shown to be an important regulator of the rod photoreceptor development (12, 13). Fundus differences observed between humans and mice might be the result of differences in RA action. It was shown that in higher primates, Müller cells contain cellular RA-binding protein (CRABP), whereas the Müller cells of rats and rabbits do not (23). Müller cells produce neurotrophins that are important for rod photoreceptor development (14, 15, 26). RA could control the expression of neurotrophins in Müller cells of primates and not in rodents. Indeed, RA was reported to regulate expression of the ciliary neurotrophic factor (25). Hence, photoreceptor differentiation regulated through Müller cells could be different in humans and mice.

From our analysis, it is clear that at high bleaching levels, 11-*cis*-RoDH$^{-/-}$ mice have delayed dark adaption kinetics, as do humans suffering from mutations in the gene encoding 11-*cis*-RoDH (46). However, in fully dark-adapted 11-*cis*-RoDH$^{-/-}$ mice, a rod ERG response comparable to that of 11-*cis*-RoDH$^{+/+}$ mice was measured. Hence, 11-*cis*-RoDH$^{-/-}$ mice are still capable of regenerating their rod visual pigment, which means that, in addition to 11-*cis*-RoDH, another unknown enzyme(s) is able to catalyze 11-*cis*-retinol oxidation in the retina. Recently, 11-*cis*-RoDH activity was also found to be associated with plasma membrane (PM) fractions (19). 11-*cis*-RoDH, however, was found to be associated with the endoplasmic reticulum (ER) of RPE cells (39). A second enzyme capable of 11-*cis*-retinol oxidation is therefore likely to be

present in the PM of RPE cells. 11-*cis*-Retinyl ester hydrolase activity was also found to be present within the PM (20). 11-*cis*-Retinal biosynthesis could therefore occur both in the ER and at the PM. Loss of 11-*cis*-retinol oxidation capacity in the ER of 11-*cis*-RoDH$^{-/-}$ mice resulted in a 50-fold increase in the *cis*-retinyl ester concentration. The 11-*cis*-retinyl ester and 11-*cis*-retinyl ester hydrolase were shown to colocalize in the RPE PM (18). A high 11-*cis*-retinyl ester concentration in the PM of 11-*cis*-RoDH$^{-/-}$ mice could prove to be a better subcellular locale for production of 11-*cis*-retinal in mice than in humans. Hence, in different species the relative contribution to 11-*cis*-retinal biosynthesis by each of the two subcellular compartments could be different. This is also emphasized by the observation that at bleaching levels at which patients suffering from fundus albipunctatus can be diagnosed unequivocally, 11-*cis*-RoDH$^{-/-}$ mice still show normal dark adaptation kinetics.

Recent studies in humans show that lack of retinol-binding protein in serum progressively affects both retinal morphology and function (36). However, young mice lacking serum retinol-binding protein (SRBP) have abnormal ERGs that become normal by 5 months of age (30). It was suggested that in mice, SRBP functions to store vitamin A and is necessary to release retinol from hepatic retinol stores. A phenotype with regard to retinal function therefore only became overt when the SRBP knockout animals were placed on a vitamin A-deficient diet. Hence, unlike humans, mice with retinol-binding protein deficiency develop a normal functioning retina, although at a slower pace than their wild-type littermates. Also, the structure of the retina in SRBP-deficient mice is reported to be normal, whereas humans develop atrophic RPE and focal loss of RPE in addition to macular pathology. Hence, SRBP-deficient mice do not phenotypically mimic the disease phenotype observed in humans. Both the 11-*cis*-RoDH and SRBP knockout mouse models suggest that mice are better able to adapt or make use of different metabolic routes for retinoid metabolism than humans, resulting in less pronounced retinal pathology.

ACKNOWLEDGMENTS

We thank W. van den Broek and F. Oerlemans for helpful discussions.

We acknowledge the technical support of the Central Animal Laboratory of the University of Nijmegen. This work was supported by grants from the following foundations: Rotterdamse Vereniging Blindenbelangen, Stichting Blindenhulp, and Deutsche Forschungsgemeinschaft (Ru 457/6-3). This research was further supported by NIH grant EY09339 (K.P.), an award from Research to Prevent Blindness, Inc. (R.P.B.), to the Department of Ophthalmology at the University of Washington, and the E. K. Bishop Foundation. K.P. is a Bishop Professor.

REFERENCES

1. **Bernstein, P. S., W. C. Law, and R. R. Rando.** 1987. Isomerization of all-*trans*-retinoids to 11-*cis*-retinoids. Proc. Natl. Acad. Sci. USA **84:**1849–1853.
2. **Chai, X., Y. Zhai, and J. L. Napoli.** 1997. cDNA cloning and characterization of a *cis*-retinol/3α-hydroxysterol short-chain alcohol dehydrogenase. J. Biol. Chem. **272:**33125–33131.
3. **Dolle, P., V. Fraulob, P. Kastner, and P. Chambon.** 1994. Developmental expression of murine retinoid X receptor (RXR) genes. Mech. Dev. **45:**91–104.
4. **Driessen, C. A. G. G., A. P. M. Janssen, H. J. Winkens, A. H. M. Van Vugt, A. L. M. De Leeuw, and J. J. M. Janssen.** 1995. Cloning and expression of a cDNA encoding bovine retinal pigment epithelial 11-*cis*-retinol dehydrogenase. Invest. Ophthalmol. Vis. Sci. **36:**1988–1996.
5. **Driessen, C. A. G. G., H. J. Winkens, E. D. Kuhlmann, A. P. M. Janssen, A. H. M. Van Vugt, A. F. Deutman, and J. J. M. Janssen.** 1997. Cloning and structural analysis of the murine *GCN5L1* gene. Gene **208:**27–31.
6. **Driessen, C. A. G. G., H. J. Winkens, E. D. Kuhlmann, A. P. M. Janssen, A. H. M. Van Vugt, A. F. Deutman, and J. J. M. Janssen.** 1998. The visual cycle retinol dehydrogenase: possible involvement in the 9-*cis*-retinoic acid pathway. FEBS Lett. **428:**135–140.
7. **Goto, Y., N. S. Peachey, H. Ripps, and M. I. Naash.** 1995. Functional abnormalities in transgenic mice expressing a mutant rhodopsin gene. Invest. Ophthalmol. Vis. Sci. **36:**62–71.
8. **Gu, S., D. A. Thompson, S. Srikumari, B. Lorenz, U. Finckh, A. Nicoletti, K. R. Murthy, M. Rathmann, G. Kumaramanickavel, M. J. Denton, and A. Gal.** 1997. Mutations in RPE65 cause autosomal recessive childhood-onset severe retinal dystropy. Nat. Genet. **17:**194–197.
9. **Humphries, M. M., D. Rancourt, G. J. Farrar, P. Kenna, M. Hazel, R. A. Bush, P. A. Sieving, D. M. Sheils, N. McNally, P. Creighton, A. Erven, A. Boros, K. Gulya, M. R. Capecchi, and P. Humphries.** 1997. Retinopathy induced in mice by targeted disruption of the rhodopsin gene. Nat. Genet. **15:**216–219.
10. **Janssen, J. J. M., A. P. M. Janssen, and A. H. M. Van Vugt.** 1994. Characterization of monoclonal antibodies recognizing retinal pigment epithelial antigens. Invest. Ophthalmol. Vis. Sci. **35:**189–198.
11. **Janssen, J. J. M., E. D. Kuhlmann, A. H. M. Van Vugt, H. J. Winkens, A. P. M. Janssen, A. F. Deutman, and C. A. G. G. Driessen.** 1999. Retinoic acid receptors and retinoid X receptors in the mature retina: subtype determination and cellular distribution. Curr. Eye Res. **19:**338–347.
12. **Kelley, M. W., J. K. Turner, and T. A. Reh.** 1994. Retinoic acid promotes differentiation of photoreceptors in vitro. Development **120:**2091–2102.
13. **Kelley, M. W., R. C. Williams, J. K. Turner, J. M. Creech-Kraft, and T. A. Reh.** 1999. Retinoic acid promotes rod photoreceptor differentiation in rat retina in vivo. Neuroreport **10:**2389–2394.
14. **Kirsch, M., M. Y. Lee, V. Meyer, A. Wiese, and H. D. Hofmann.** 1997. Evidence for multiple, local functions of ciliary neurotrophic factor (CNTF) in retinal development: expression of CNTF and its receptors and in vitro effects on target cells. J. Neurochem. **68:**979–990.
15. **Kirsch, M., S. Schulz-Key, A. Wiese, S. Fuhrmann, and H. Hofmann.** 1998. Ciliary neurotrophic factor blocks rod photoreceptor differentiation from postmitotic precursor cells in vitro. Cell Tissue Res. **291:**207–216.
16. **Lem, J., N. V. Krasnoperova, P. D. Calvert, B. Kosaras, D. A. Cameron, M. Nicolo, C. L. Makino, and R. L. Sidman.** 1999. Morphological, physiological, and biochemical changes in rhodopsin knock-out mice. Proc. Natl. Acad. Sci. USA **96:**736–741.
17. **Liou, G. I., Y. Fei, N. S. Peachey, S. Matragoon, S. Wei, W. S. Blaner, Y. Wang, C. Liu, M. E. Gottesman, and H. Ripps.** 1998. Early onset photoreceptor abnormalities induced by targeted disruption of the interphotoreceptor retinoid-binding protein gene. J. Neurosci. **18:**4511–4520.
18. **Marlhens, F., C. Bareil, J. Griffoin, E. Zrenner, P. Amalric, C. Eliaou, S. Liu, E. Harris, T. M. Redmond, B. Arnaud, M. Claustress, and C. P. Hamel.** 1997. Mutations in *RPE65* cause Leber's congenital amaurosis. Nat. Genet. **17:**139–141.
19. **Mata, N. L., and A. T. Tsin.** 1998. Distribution of 11-cis LRAT, 11-cis RD and 11-cis REH in bovine retinal pigment epithelium membranes. Biochim. Biophys. Acta **1394:**16–22.
20. **Mata, N. L., E. T. Villazana, and A. T. Tsin.** 1998. Colocalization of 11-cis retinyl esters and retinyl ester hydrolase activity in retinal pigment epithelium plasma membrane. Invest. Ophthalmol. Vis. Sci. **39:**1312–1319.
21. **Maw, M. A., B. Kennedy, A. Knight, R. Bridges, K. E. Roth, E. J. Mani, J. K. Mukkadan, D. Nancarrow, J. W. Crabb, and M. J. Denton.** 1997. Mutation of the gene encoding cellular retinaldehyde binding protein in autosomal recessive retinitis pigmentosa. Nat. Genet. **17:**198–200.
22. **Mertz, J. R., E. Shang, R. Piantedosi, S. Wei, D. J. Wolgemuth, and W. S. Blaner.** 1997. Identification and characterization of a stereospecific human enzyme that catalyzes 9-*cis*-retinol oxidation: a possible role in 9-*cis*-retinoic acid formation. J. Biol. Chem. **272:**11744–11749.
23. **Milam, A. H., A. M. De Leeuw, V. P. Gaur, and J. C. Saari.** 1990. Immunolocalization of cellular retinoic acid binding protein to Müller cells and/or a subpopulation of GABA-positive amacrine cells in retinas of different species. J. Comp. Neurol. **296:**123–129.
24. **Morimura, H., G. A. Fishmann, S. A. Grover, A. B. Fulton, E. L. Berson, and T. P. Dryja.** 1998. Mutations in the RPE65 gene in patients with autosomal recessive retinitis pigmentosa or Leber congenital amaurosis. Proc. Natl. Acad. Sci. USA **95:**3088–3093.
25. **Nakanishi, T., K. Ishii, N. Fukushima, M. Asanuma, E. Iwata, and N. Ogawa.** 1996. Expression of mRNA encoding neurotrophic factors and its regulation in a hybrid neuronal cell line. Biochem. Mol. Biol. Int. **38:**763–772.
26. **Neophytou, C., A. B. Vernallis, A. Smith, and M. C. Raff.** 1997. Müller-cell-derived leukaemia inhibitory factor arrests rod photoreceptor differentiation at a postmitotic pre-rod stage of development. Development **124:**2345–2354.
27. **Niederreither, K., V. Subbarayan, P. Dolle, and P. Chambon.** 1999. Embryonic retinoic acid synthesis is essential for early mouse post-implantation development. Nat. Genet. **21:**444–448.
28. **Palczewski, K., and J. C. Saari.** 1997. Activation and inactivation steps in the visual transduction pathway. Curr. Opin. Neurobiol. **7:**500–504.
29. **Palczewski, K., J. P. VanHooser, G. G. Garwin, J. Chen, G. I. Liou, and J. C. Saari.** 1999. Kinetics of visual pigment regeneration in excised mouse eyes and in mice with a targeted disruption of the gene encoding interphotore-

ceptor retinoid-binding protein or arrestin. Biochemistry **38:**12012–12019.
30. **Quadro, L., W. S. Blaner, D. Salchow, S. Vogel, R. Piantedosi, P. Gouras, S. Freeman, M. P. Cosma, V. Colantuoni, and M. E. Gottesman.** 1999. Impaired retinal function and vitamin A availability in mice lacking retinol-binding protein. EMBO J. **18:**4633–4644.
31. **Redmond, T. M., S. Yu, E. Lee, D. Bok, D. Hamasaki, N. Chen, P. Goletz, J. X. Ma, R. K. Crouch, and K. Pfeifer.** 1998. RPE65 is necessary for production of 11-*cis*-vitamin A in the retinal visual cycle. Nat. Genet. **20:**344–351.
32. **Romert, A., P. Tuvendal, A. Simon, L. Dencker, and U. Eriksson.** 1998. The identification of a 9-*cis*-retinol dehydrogenase in the mouse embryo reveals a pathway for synthesis of 9-*cis*-retinoic acid. Proc. Natl. Acad. Sci. USA **95:** 4404–4409.
33. **Saari, J. C., and D. L. Bredberg.** 1987. Photochemistry and stereoselectivity of cellular retinaldehyde-binding protein from bovine retina. J. Biol. Chem. **262:**7618–7622.
34. **Saari, J. C., G. G. Garwin, J. P. Van Hooser, and K. Palczewski.** 1998. Reduction of all-*trans*-retinal limits regeneration of visual pigment in mice. Vision Res. **38:**1325–1333.
35. **Saari, J. C., G. G. Garwin, F. Haeseleer, G.-F. Jang, and K. Palczewski.** 2000. Phase partition and high-performance liquid chromatography assays of retinoid dehydrogenases. Methods Enzymol. **316:**359–371.
36. **Seeliger, M. W., I. Frank, S. Beck, and E. Zrenner.** 1999. Phenotype in retinol deficiency due to a hereditary defect in retinol binding protein biosynthesis. Invest. Ophthalmol. Vis. Sci. **40:**3–11.
37. **Simon, A., U. Hellman, C. Wernstedt, and U. Eriksson.** 1995. The retinal pigment epithelial-specific 11-*cis*-retinol dehydrogenase belongs to the family of short chain alcohol dehydrogenase. J. Biol. Chem. **270:**1107–1112.
38. **Simon, A., J. Lagercrantz, S. Bajalica-Lagercrantz, and U. Eriksson.** 1996. Primary structure of human 11-*cis*-retinol dehydrogenase and organization and chromosomal localization of the corresponding gene. Genomics **36:**424–430.
39. **Simon, A., A. Romert, A. L. Gustafson, J. M. McCaffery, and U. Eriksson.** 1999. Intracellular localization and membrane topology of 11-cis retinol dehydrogenase in the retinal pigment epithelium suggest a compartmentalized synthesis of 11-*cis* retinaldehyde. J. Cell Sci. **112:**549–558.
40. **Stecher, H., M. H. Gelb, J. C. Saari, and K. Palczewski.** 1999. Preferential release of 11-*cis*-retinol from retinal pigment epithelial cells in the presence of cellular retinaldehyde-binding protein. J. Biol. Chem. **274:**8577–8585.
41. **Su, J., X. Chai, B. Kahn, and J. L. Napoli.** 1998. cDNA cloning, tissue distribution, and substrate characteristics of a *cis*-retinol/3α-hydroxysterol short-chain dehydrogenase isozyme. J. Biol. Chem. **273:**17910–17916.
42. **Wang, J., X. Chai, U. Eriksson, and J. L. Napoli.** 1999. Activity of human 11-*cis*-retinol dehydrogenase (Rdh5) with steroids and retinoids and expression of its mRNA in extra-ocular human tissue. Biochem. J. **338:**23–27.
43. **Wendling, O., P. Chambon, and M. Mark.** 1999. Retinoid X receptors are essential for early mouse development and placentogenesis. Proc. Natl. Acad. Sci. USA **96:**547–551.
44. **Weng, J., N. L. Mata, S. M. Azarian, R. T. Tzekov, D. G. Birch, and G. H. Travis.** 1999. Insights into the function of rim protein in photoreceptors and etiology of Stargardt's disease from the phenotype in *abcr* knockout mice. Cell **98:**13–23.
45. **Winston, A., and R. R. Rando.** 1998. Regulation of isomerohydrolase activity in the visual cycle. Biochemistry **37:**2044–2050.
46. **Yamamoto, H., A. Simon, U. Eriksson, E. Harris, E. L. Berson, and T. P. Dryja.** 1999. Mutations in the gene encoding 11-*cis*-retinol dehydrogenase cause delayed dark adaptation and fundus albipunctatus. Nat. Genet. **22:** 188–191.
47. **Yang, R. B., S. W. Robinson, W. H. Xiong, K. W. Yau, D. G. Birch, and D. L. Garbers.** 1999. Disruption of a retinal guanylyl cyclase gene leads to cone-specific dystrophy and paradoxical rod behavior. J. Neurosci. **19:**5889–5897.
48. **Zimmerman, W. F., F. Lion, F. J. M. Daemen, and S. L. Bonting.** 1975. Biochemical aspects of the visual process. XXX. Distribution of stereospecific dehydrogenase activities in subcellular fractions of the bovine retina and pigment epithelium. Exp. Eye Res. **21:**325–332.